Multi-layer, offset-coupled sapphire fiber Bragg gratings for high-temperature measurements

Xizhen Xu,[1,2] **Jun He,**[1,2,*] **Changrui Liao,**[1,2] **and Yiping Wang**[1,2]

[1]*Key Laboratory of Optoelectronic Devices and Systems of Ministry of Education and Guangdong Province, College of Physics and Optoelectronic Engineering, Shenzhen University, Shenzhen 518060, China*
[2]*Guangdong and Hong Kong Joint Research Centre for Optical Fiber Sensors, Shenzhen University, Shenzhen 518060, China*
Corresponding author: hejun07@szu.edu.cn

We demonstrate the fabrication of multi-layer sapphire fiber Bragg gratings (SFBGs) using a femtosecond laser line-by-line scanning technique. This multi-layer grating structure enlarges the index modulation area and can effectively increase the reflectivity of SFBGs. The spectral characteristics of multi-layer SFBGs with different layer quantities and spacings were studied. A double-layer SFBG with a layer spacing of 5 µm exhibits a reflectivity of 34.1%, which is much higher than that of a single-layer SFBG (i.e., ~6.3%). Moreover, the higher-order modes of multi-layer SFBG could be suppressed by offset coupling, leading to a reduced SFBG bandwidth (full width at half-maximum [FWHM]) of 1.32 nm. In addition, the high-temperature response of the multi-layer, offset-coupled SFBGs was also studied. The SFBG can withstand a high temperature of 1612°C and exhibits a sensitivity of 45.2 pm/°C at high temperatures. Such multi-layer, offset-coupled SFBGs could be developed for high-temperature sensing in metallurgical, chemical, and aviation industries.   © 2019 Optical Society of America

High-temperature measurements are critical in many engineering fields such as metallurgical, chemical, and aviation industries. For example, sensing in aero engines needs to endure high operating temperatures of up to 1800°C. However, conventional silica-based fiber Bragg gratings (FBGs) only can withstand temperatures of up to 1300°C due to the glass transition temperature of silica ($Tg \approx 1330°C$) [1,2]. Bragg gratings fabricated in single-crystal sapphire fibers have been shown to withstand temperatures up to 1745°C [3], as the melting temperature of sapphire is ~2045°C [4–14]. The femtosecond laser is suitable for creating FBGs in sapphire fibers, which have no photosensitivity. The femtosecond laser scanning-beam phase mask technique has previously been proposed for fabricating sapphire fiber Bragg gratings (SFBGs) with reflectivity of up to 50% [9]. However, the Bragg wavelength of SFBGs was fixed by the phase mask period and, hence, it is difficult to use only one phase mask to fabricate a wavelength-division-multiplexed (WDM) SFBG array. After that, a femtosecond laser Talbot interferometer was

constructed, and a serial array consisting of three SFBGs at different wavelengths was successfully fabricated using this method [10]. Nevertheless, this facility requires high stability and accuracy. In 2018, a femtosecond laser point-by-point inscription method was proposed for creating a WDM SFBG array. However, the reflectivity of SFBGs inscribed using this method is extremely low (~0.6%) due to the small index modulation area formed by a single-laser pulse [12]. Additionally, all of the above-mentioned SFBGs exhibit a large bandwidth of ~6 nm in their reflection spectra [5,9–12]. The broad reflection peaks of SFBGs are induced by the multimode operation in sapphire fiber, which typically has a core diameter of over tens of microns and has no cladding layer. A large bandwidth of SFBG is disadvantageous to high-accuracy wavelength demodulation.

To date, two different methods, i.e., the tapered fiber coupling and wet-hot acid etching, have been proposed to reduce the SFBG bandwidth [6,13]. An SFBG bandwidth of 0.33 nm can be achieved using a tapered fiber coupling technique [6]. However, this method needs precise alignment and is inconvenient for practical use. In addition, a wet-hot acid etching technique was proposed to reduce the diameter of an SFBG to 9.6 µm. A smaller fiber diameter can lead to less optical modes and, hence, results in a reduced bandwidth of SFBG. However, this process is time-consuming, requiring an etching time of tens of hours [13]. Recently, we reported on the fabrication of SFBGs with a femtosecond laser line-by-line scanning technique. An SFBG inscribed using this method exhibits a low reflectivity of 6.3% and a large bandwidth of 6.08 nm [14].

In this Letter, we fabricate multi-layer FBGs in sapphire fibers using the femtosecond laser line-by-line scanning technique. The reflectivity of SFBGs can be increased effectively, since the index modulation area formed by a multi-layer structure is much larger than that formed by a single-layer structure. The influence of layer spacings and layer quantities were studied. After optimizing these parameters, an SFBG was produced with a reflectivity of 34.1%. Subsequently, a reduced −3 dB bandwidth of 1.32 nm was achieved in the SFBG using offset coupling. The higher order modes can be suppressed by this means. Then the high-temperature response of these multi-layer SFBGs was also investigated. The results show that the device could withstand a high temperature of up to 1612°C,

exhibiting a temperature sensitivity of 45.2 pm/°C at the high-temperature region. The high-temperature response of the multi-layer SFBGs is consistent with the single-layer SFBGs.

We used a frequency-doubled regenerative amplified Yb:KGW (KGd(WO3)) femtosecond laser (Pharos, Light Conversion) with a wavelength of 514 nm, a pulse width of 290 fs, and a repetition rate of 200 kHz for fabricating the multi-layer SFBGs. The laser beam was focused by a 63× Zeiss oil-immersion objective with a numerical aperture of 1.40 into the sapphire fiber. The aberration at the sapphire/air interface can be reduced by applying refractive index matching oil. A commercial sapphire optical fiber (MicroMaterials Inc.) was mounted on an assembled three-dimensional translation stage (Aerotech ABL15010, ANT130LZS, and ANT130V-5).

The fabrication process of multi-layer SFBGs is shown in Fig. 1. As shown in Fig. 1(a), the axial direction of the sapphire fiber was parallel to the translation along z-axis. The shutter was opened, and the femtosecond laser beam was focused into the sapphire fiber. The sapphire fiber was first translated along the x-axis (blue line) at a constant speed v_1 with a distance of a. Hence, the first line with a track length of a was inscribed. Then, as shown in Fig. 1(c), the sapphire fiber was translated along a diagonal line (green dashed line) at a constant speed v_2 via synchronous movements along the x-axis and y-axis. The shutter was closed during this step to prevent laser inscription. Subsequently, as shown in Fig. 1(c), the shutter was reopened, and the second line with the same track length of a was inscribed by translation along the x-axis (blue line) at the same speed v_1. As the lateral view shown in Fig. 1(b), the index modulation lines l_1 and l_2 constitute a grating plane of the SFBG. Then, as shown in Fig. 1(a), the sapphire fiber was first translated back to the upper layer and then translated along a diagonal line (green dot line) at a constant speed v_2. The shutter was closed again in this step. The subsequent grating planes (i.e., formed by multiple lines) were sequentially inscribed by repeating the previous process. The line spacing along z-axis was set to Λ, as shown in Fig. 1(a). Hence, a Bragg grating with a track length of a, grating pitch of Λ, grating pitch quantity of N, layer spacing of d, and layer quantity of M, was formed by these lines inscribed in a sapphire fiber.

Bragg gratings were fabricated in a 60 μm diameter sapphire fiber. In the fabrication process, a single-pulse energy of 32.5 nJ was employed with translation speeds v_1 and v_2 of 0.2 mm/s, track length a of 40 μm, grating pitch Λ of 1.78 μm, grating pitch quantity N of 1126, and grating length L of ~2 mm. A tunable laser source (Keysight, 81940A), an optical power meter (Keysight, N7744A), and a multimode fiber (MMF) coupler (62.5/125 μm, 50:50) were used to record the reflection spectra of SFBGs with a resolution of 6 pm.

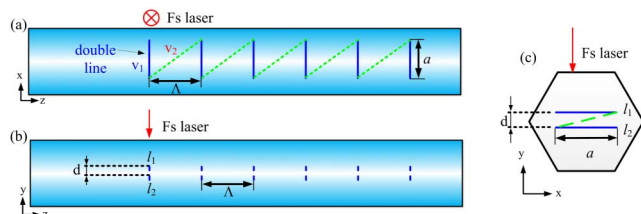We fabricated four double-layer SFBGs (S1-S4) with decreasing layer spacings of 9, 7, 5, and 3 μm, respectively.

Note that the time for fabricating such an SFBG was ~15 min. The cross-sectional- and lateral-view microscope images of these SFBGs were shown in Figs. 2(a1)–2(a4) and 2(b1)–2(b4), respectively. The length, width, depth, and line spacing of these laser-inscribed grating lines were measured to be 41.10, 1.03, 5.01, and 1.78 μm, respectively. The corresponding reflection spectra of these SFBGs are shown in Figs. 2(c1)–2(c4). SFBGs S1-S4 have a fourth-order Bragg wavelength of 1552.62, 1551.92, 1554.25, and 1553.72 nm, a signal-to-noise ratio (SNR) of 6.74, 10.95, 15.51, and 3.44 dB, a –3 dB bandwidth (FWHM) of 6.20, 2.61, 1.74, and 7.60 nm, respectively. Note that the SFBG with a layer spacing of 5 μm (i.e., S3) has the highest reflectivity and the narrowest bandwidth.

The measured peak reflectivity $R(\lambda_i)$ of a multimode SFBG can be expressed as [15,16]

$$R(\lambda_i) = \eta(\lambda_i) \cdot \tanh^2(\kappa_i \cdot L), \quad (1)$$

where λ_i is the wavelength of reflection peak, L is the SFBG length, κ_i is the grating strength of the ith guided modes, $\eta(\lambda_i)$ is the mode coupling efficiency, i.e., the percentage of the total power that is distributed into the ith guided mode, which couples with each other and generates the reflection peak. $\eta(\lambda_i)$ is determined by [17]

$$\eta(\lambda_i) = \frac{\left| \int_0^\infty E_0(r)E_i(r)r\mathrm{d}r \right|^2}{\int_0^\infty |E_0(r)|^2 r\mathrm{d}r \cdot \int_0^\infty |E_i(r)|^2 r\mathrm{d}r}, \quad (2)$$

where E_0 and E_i represent the field distributions of the input mode and the ith guided mode, respectively. The grating strength κ_i of the SFBG could be expressed as [18]

$$\kappa_i = \frac{\pi}{\lambda_i} \int_{-\infty}^\infty \int_{-\infty}^\infty \Delta n(x,y)E_i(x,y)E_i^*(x,y)\mathrm{d}x\mathrm{d}y, \quad (3)$$

where $\Delta n(x,y)$ is the refractive index modulation region formed by femtosecond laser multi-layer line-by-line inscription. Moreover, it could be deduced from Eq. (3) that the grating strength of an SFBG depends not only on the refractive
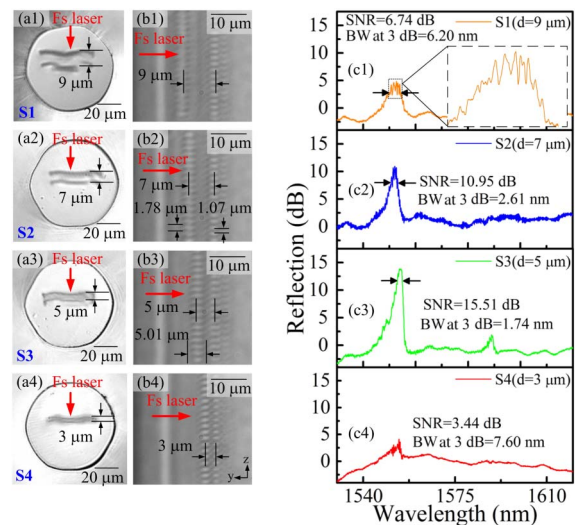

Fig. 2. Four SFBGs S1-S4 inscribed with decreasing layer spacings of 9, 7, 5, and 3 μm, respectively. (a) Cross-sectional- and (b) lateral-view microscope images of the SFBGs S1, S2, S3, and S4; (c) corresponding reflection spectra of SFBGs S1-S4.

Fig. 1. Schematics of fabricating multi-layer SFBGs: (a) top view, (b) lateral view, and (c) cross-sectional view.

index modulation depth Δn, but also on the overlap between the index modulation area and mode field distributions [19,20]. This means the peak reflectivity of the SFBG can be increased by enlarging the index modulation area (i.e., using a plane consisting of multiple lines in a multi-layer SFBG to substitute the single line in a conventional single-layer SFBG). In addition, the bandwidth of the SFBG can be reduced by selectively increasing the overlap between the index modulation area and lower-order modes, most of which are located in the sapphire fiber center.

In the case of a double-layer SFBG with a layer spacing of 5 μm (i.e., S3), as shown in Figs. 2(a3) and 2(b3), there is neither overlap nor gap between the two inscribed layers, since the layer spacing could be comparable to the focal depth of the incident laser beam. This results in a doubled index modulation area and, hence, significantly increases the grating strength κ_i of the lower-order modes in the SFBG. It is clear from Eq. (1) that a larger grating strength leads to a higher grating reflectivity of the SFBG. In the case of a double-layer SFBG with a smaller layer spacing of 3 μm (i.e., S4), as shown in Figs. 2(a4) and 2(b4), an overlap exists between the two inscribed layers. The index modulation induced by the first layer could be modified or even partially erased by the second layer, leading to a smaller index modulation area in S4 than that in S3. Hence, it is observed from Fig. 2(c4) that the reflectivity and the SNR of SFBG S4 decease drastically with a reduced layer spacing. Additionally, in the case of a double-layer SFBG with a larger layer spacing of 7 μm (i.e., S2), as shown in Figs. 2(a2) and 2(b2), a gap exists between the two layers. The resulting index modulation area includes unaffected regions in the center. As a result, the overlap between the lower-order mode fields and index modulation area formed in S2 is smaller than that formed in S3. This results in a smaller grating strength, a reduced grating reflectivity, and a reduced SNR, as shown in Figs. 2(c2). In the case of a double-layer SFBG with a larger layer spacing of 9 μm (i.e., S1), as shown in Figs. 2(a1) and 2(b1), the gap between the two inscribed layers is even larger. Hence, the grating reflectivity and SNR are further reduced, as shown in Fig. 2(c1). In addition, the reflection peak of SFBG S1 splits into multiple peaks, as shown in the inset of Fig. 2(c1). This indicates that the quantity of modes in the SFBG decreases as a few-mode optical waveguide was probably formed between the two laser-inscribed layers [13,21].

Subsequently, we fabricated three SFBGs with different layer quantities of 1, 2, and 3 (i.e., single-layer, double-layer, and triple-layer SFBGs). Each SFBG has the same grating pitch of 1.78 μm, the same track length of 40 μm, and the same

grating length of ∼2 mm. Moreover, the double-layer and triple-layer SFBGs have the same layer spacing of 5 μm. The cross-sectional-view and lateral-view microscope images of the SFBGs with layer quantities of 1, 2, and 3 are shown in Figs. 3(a1)–3(a3) and Figs. 3(b1)–3(b3), respectively. As the reflection spectra of these SFBGs shown in Fig. 3(c), the SNRs of the reflection peaks of single-layer, double-layer, and triple-layer SFBGs are 10.50, 15.51, and 9.71 dB, respectively (i.e., the double-layer SFBG has the highest SNR, whereas the triple-layer SFBG has a similar SNR to the single-layer SFBG). As shown in Figs. 3(a2) and 3(a3), the index modulation area formed in the triple-layer SFBG is much larger than that in the double-layer SFBG. Hence, the triple-layer SFBG should have a higher reflectivity and SNR. However, as shown in Fig. 3(c), the triple-layer SFBG has a lower reflectivity and SNR than the double-layer SFBG. In addition, the peak wavelength of the triple-layer SFBG is shorter than that of the single-layer SFBG and double-layer SFBG. This indicates a complex index modulation area was formed in the triple-layer SFBG, and the grating strength of the lower-order modes was reduced.

We also investigated the effect of lateral offset coupling between the launch fiber and the multi-layer SFBG on the reflection spectra. A double-layer SFBG with a grating pitch of 1.78 μm, track length of 40 μm, layer spacing of 5 μm, and pitch quantity of 1126 was fixed onto a fiber holder of a fusion splicer (Fujikura, FSM-100P+), along with a launch MMF (62.5/125 μm) fixed onto the other fiber holder. A series of lateral offsets in two orthogonal directions can be applied using the x-axis motor and y-axis motor in the splicer. At first, the SFBG was aligned to the launch fiber and rotated in the splicer to ensure that the laser-inscribed lines were along the x-axis. Then, as shown in Fig. 4(a1), the SFBG was translated vertically from 0 to 25 μm with a step of 1 μm along the y-axis. After that, the SFBG was moved backward to its original position. Subsequently, as shown in Fig. 4(a2), the SFBG was translated horizontally from 0 to 25 μm with a step of 1 μm along the x-axis. The corresponding reflection spectra of offset-coupled SFBGs were recorded during the x/y translation process.

In case the double-layer SFBG was aligned to the launch MMF (i.e., coupled with no offset), as shown in the green line
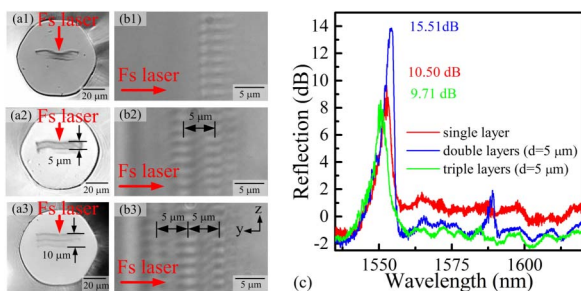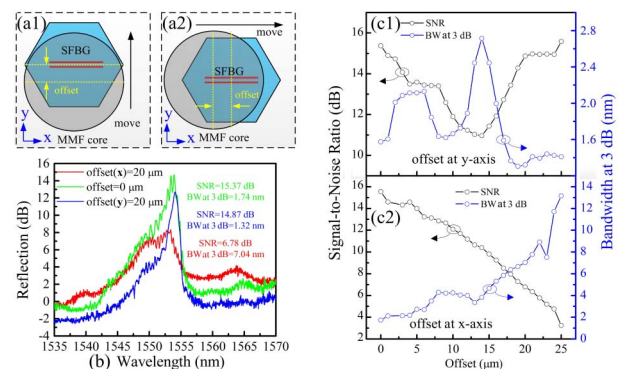

Fig. 3. Three SFBGs inscribed with increasing layer quantities of 1, 2, and 3, respectively. (a) Cross-sectional-view and (b) lateral-view microscope images of single-layer, double-layer, and triple-layer SFBGs; (c) corresponding reflection spectra of these SFBGs.

Fig. 4. Schematics of the double-layer SFBG offset-coupled with a launch MMF along (a1) the y-axis and (a2) the x-axis. (b) Reflection spectra of a double-layer SFBG-coupled with no offset (0 μm), 20 μm offset along the y-axis, and 20 μm offset along the x-axis. The evolutions of SNRs and bandwidths in the reflection spectra of a offset-coupled double-layer SFBG as functions of applied offsets varied from 0 to 25 μm along (c1) the y-axis and (c2) the x-axis.

in Fig. 4(b), a maximum SNR of 15.37 dB and a –3 dB bandwidth of 1.74 nm were obtained. In this case, both lower-order modes and higher-order modes could be excited efficiently. In case the double-layer SFBG was offset-coupled with an increasing offset along the y-axis (i.e., perpendicular to the laser-inscribed lines), as shown in Figs. 4(a1) and 4(c1), the SNR decreases at first, and then recovers to its original value gradually, whereas the bandwidth increases at first, and then decreases. As shown in the blue line in Fig. 4(b), the reflectivity and the SNR of the higher-order modes (i.e., spectral components in shorter wavelengths) decrease drastically, whereas the reflectivity and the SNR of the lower-order modes (i.e., spectral components in longer wavelengths) decrease slightly. As a result, a narrower bandwidth of 1.32 nm and a slightly lower SNR of 14.87 dB were obtained in the double-layer SFBG-coupled with a 20 µm -offset along the y-axis. Additionally, in case the double-layer SFBG was offset-coupled with an increasing offset along the x-axis (i.e., along the laser-inscribed lines), as shown in Figs. 4(a2) and 4(c2), the SNR decreases, while the bandwidth increases drastically. As shown in the red line in Fig. 4(b), the reflectivity and the SNR of the lower-order modes decrease drastically, whereas the reflectivity and the SNR of the higher-order modes are almost unchanged. As a result, a larger –3 dB bandwidth of 7.04 nm and a much lower SNR of 6.78 dB were obtained in the double-layer SFBG-coupled with a 20 µm offset along the x-axis. The measured grating reflectivity of different modes in the SFBG depends on each grating strength κ_i and coupling efficiency $\eta(\lambda_i)$. As a result, the spectral shape of SFBG was affected by offset coupling, since $\eta(\lambda_i)$ of different modes was unevenly changed by lateral offsets. In additional, the directional response results from the near rectangular index modulation profile created by these laser-inscribed lines. Therefore, the lateral offset coupling applied on a double-layer SFBG along the orthogonal direction to the laser-inscribed tracks could be used to suppress the higher-order modes and reduce the bandwidth of the SFBG.

Furthermore, the temperature response of a double-layer SFBG was investigated using a tube furnace (Carbolite, Gero HTRH). The temperature in the furnace was cycled from room temperature to 1612°C at a step of ~100°C, being maintained for 20 min at each measurement point to assure the stability of the reflection spectra. A B-type thermocouple was placed along the SFBG to record the temperature. The complete temperature response of the double-layer SFBG from room temperature up to 1612°C is demon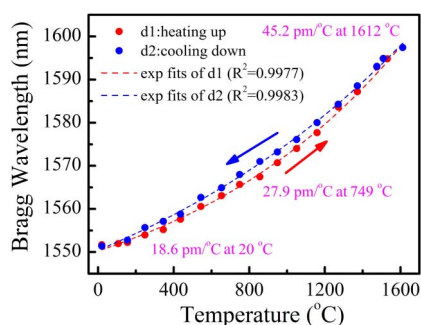strated in Fig. 5. The sensitivities at various temperatures, i.e., 18.6 pm/°C at 20°C, 27.9 pm/°C at 749°C, and 45.2 pm/°C at 1612°C, were evaluated by applying exponential fits to the measured data. Note that the sensitivity increases at elevated temperatures. This should result from a larger thermal-optic coefficient of sapphire fiber and a changing relative strength of the various modal contributions.

In summary, we fabricated multi-layer SFBGs via a femtosecond laser line-by-line scanning. The reflection spectra of the SFBGs with varying layer spacings and layer quantities were investigated. A double-layer SFBG with a reflectivity of 34.1% and a –3 dB bandwidth of 1.74 nm was achieved. Moreover, lateral offset coupling along the orthogonal direction to the laser-inscribed tracks was used to suppress the higher-order modes in SFBGs, leading to a reduced –3 dB bandwidth of 1.32 nm. A high-temperature test demonstrates that the double-layer SFBG can operate at 1612°C with a sensitivity of 45.2 pm/°C. Hence, such multi-layer, offset-coupled SFBGs could be developed for promising high-temperature sensors in metallurgical, chemical, and aviation industries.

Fig. 5. Bragg wavelength of a double-layer SFBG as a function of the temperature in the case of temperature cycling from 20°C to 1612°C.

REFERENCES

1. C. R. Liao and D. N. Wang, Photonics Sens. **3**, 97 (2013).
2. J. He, Y. P. Wang, C. R. Liao, C. Wang, S. Liu, K. M. Yang, Y. Wang, X. C. Yuan, G. P. Wang, and W. J. Zhang, Sci. Rep. **6**, 23379 (2016).
3. M. Busch, W. Ecke, I. Latka, D. Fischer, R. Willsch, and H. Bartelt, Meas. Sci. Technol. **20**, 115301 (2009).
4. B. Liu, Z. H. Yu, C. Hill, Y. J. Cheng, D. Homa, G. Pickrell, and A. B. Wang, Opt. Lett. **41**, 4405 (2016).
5. D. Grobnic, S. J. Mihailov, C. W. Smelser, and H. M. Ding, IEEE Photonics Technol. Lett. **16**, 2505 (2004).
6. D. Grobnic, S. J. Mihailov, H. Ding, F. Bilodeau, and C. W. Smelser, Meas. Sci. Technol. **17**, 980 (2006).
7. S. J. Mihailov, D. Grobnic, and C. W. Smelser, Opt. Lett. **35**, 2810 (2010).
8. Z. P. Tian, Z. H. Yu, B. Liu, and A. B. Wang, Opt. Lett. **41**, 195 (2016).
9. C. Chen, X. Y. Zhang, Y. S. Yu, W. H. Wei, Q. Guo, L. Qin, Y. Q. Ning, L. J. Wang, and H. B. Sun, J. Lightwave Technol. **36**, 3302 (2018).
10. T. Elsmann, T. Habisreuther, A. Graf, M. Rothhardt, and H. Bartelt, Opt. Express **21**, 4591 (2013).
11. T. Habisreuther, T. Elsmann, Z. W. Pan, A. Graf, R. Willsch, and M. A. Schmidt, Appl. Therm. Eng. **91**, 860 (2015).
12. S. Yang, D. Hu, and A. B. Wang, Opt. Lett. **42**, 4219 (2017).
13. S. Yang, D. Homa, G. Pickrell, and A. B. Wang, Opt. Lett. **43**, 62 (2018).
14. X. Z. Xu, J. He, C. R. Liao, K. M. Yang, K. K. Guo, C. Li, Y. F. Zhang, Z. B. Ouyang, and Y. P. Wang, Opt. Lett. **43**, 4562 (2018).
15. T. Erdogan, J. Lightwave Technol. **15**, 1277 (1997).
16. H. G. Yu, Y. Wang, Q. Y. Xu, and C. Q. Xu, J. Lightwave Technol. **24**, 1903 (2006).
17. W. Mohammed, A. Mehta, and E. G. Johnson, J. Lightwave Technol. **22**, 469 (2004).
18. C. G. Lu and Y. P. Cui, J. Lightwave Technol. **24**, 598 (2006).
19. G. Bharathan, T. T. Fernandez, M. Ams, R. I. Woodward, D. D. Hudson, and A. Fuerbach, Opt. Lett. **44**, 423 (2019).
20. Y. P. Wang, Z. L. Li, S. Liu, C. L. Fu, Z. Y. Li, Z. Zhang, Y. Wang, J. He, Z. Y. Bai, and C. R. Liao, J. Lightwave Technol. **37**, 2185 (2019).
21. V. Bharadwaj, A. Courvoisier, T. T. Fernandez, R. Ramponi, G. Galzerano, J. Nunn, M. J. Booth, R. Osellame, S. M. Eaton, and P. S. Salter, Opt. Lett. **42**, 3451 (2017).